Progress In Electromagnetics Research M, Vol. 88, 133–144, 2020

Time-Domain Analysis of Overhead Line in presence of Stratified Earth

Ayoub Lahmidi and Abderrahman Maaouni*

Abstract—The presence of the ground affects the propagation on overhead lines through a magnetically induced earth return current. Numerous researches have been conducted to study this influence by considering a homogeneous earth. In the current paper, the transient response of Multi-conductor transmission Lines (MTL) considering a lossy stratified earth is presented. Based on the finite difference time-domain (FDTD) and an improvement of the convolution integral arising from time-domain modeling of frequency-dependent conductors' parameters through the Vector Fitting (VF) algorithm, a novel numerical procedure for solution of a system of telegraph equations is presented. Many simulations are introduced to highlight the effect of soil stratification on the response of the line for a given excitation. The efficiency of an equivalent model, using an equivalent single-conductor, of a multiple conductor system is also established in this work.

1. INTRODUCTION

Electromagnetic transient calculation of overhead transmission lines is strongly influenced by ground losses. Many studies have treated this influence by calculating the earth return impedance to evaluate the ground conduction effects on transmission line propagation. Carson [1] and Pollaczek [2] have studied the impedance of a homogeneous earth without considering the displacement currents in the air and the ground. Wise in [3] has included this effect, but this influence changes when we have a stratified earth. Sunde [4] extended the solution of the earth return impedance for the case of two-layers earth, but in this approach, the effect of propagation has been neglected. A more rigorous solution has been presented by Papadopoulos et al. [5] and Nakagawa [6]. The two studies have included the effect of propagation of current, but Nakagawa has, in addition, introduced the earth return impedance for 3-layers earth in his paper.

Transient analysis of transmission lines can be dealt with either in the time-domain or in the frequency-domain. A time-domain approach allows handling in more straightforward way non-linearities in power-transmission systems such as surge arresters, transmission-line shunt parameters, saturable inductors, and fault arcs. A general way to directly obtain the time domain response of the transmission line is the use of the FDTD method [7, 8]. The derivatives in the MTL equations can be approximated by a time-space second order central finite difference scheme, and the equations can be solved in a leapfrog fashion [9]. Rachidi et al. in [10] have presented an FDTD solution of the coupling equations to calculate the lightning induced voltages in lossy transmission line above a homogeneous ground. The Sunde ground impedance is adopted in conjunction with a judicious numerical treatment of the singularity emanating from the inverse Fourier transform of the ground impedance to derive a more appropriate form of coupling equations in which there is no longer a singular term. But the use of Sunde approximation makes the result less accurate for the reason quoted in the beginning of this

Received 15 October 2019, Accepted 15 December 2019, Scheduled 14 January 2020
* Corresponding author: Abderrahman Maaouni (maaouni.fsr@gmail.com).
The authors are with the ESMAR: Team — Science of Matter and Radiation, Faculty of Science, Mohammed V University, POB. 1014, Rabat, Morocco.

section. An efficient method was proposed by Kordi et al. [11], in which they had presented an FDTD formulation capable of modeling a dispersive frequency-dependent transmission line within a circuit/system simulator taking into account the losses of a homogeneous ground. Each conductor of the line is modeled as two-port stamp which only includes resistive elements and dependent current sources.

The scope of this paper is the time-domain analysis of an overhead arrangement considering the frequency-dependent behavior of the stratified earth in the framework of the quasi-TEM approximation. The Nakagawa model for the earth return impedance solution and the FDTD method are used to characterize the transient behavior on overhead lines. The use of the FDTD method requires that all parameters must be in the time-domain including the earth return impedance. The vector fitting algorithm proposed by Gustavsen and Semlyen in [12] is employed to transform those parameters into time domain. This transformation deals with a convolution integral of impedance solution and time derivatives of currents. Moreover, in the FDTD method, the spatial resolution Δz and time step Δt must be chosen according to the following stability condition [13] (the Courant-Friedrich-Levy (CFL) condition):

$$\Delta t \leq \frac{\Delta z}{v_p} \tag{1}$$

where v_p is the maximum wave phase velocity within the MTL.

Since the problem treated in this paper involves inhomogeneous medium. The FDTD method allows a very straightforward treatment of this kind of problem compared to the method of moment (MoM), which is more efficient for the homogeneous medium. Davidson [18] gives two tables comparing the FDTD, MoM, and the finite elements FEM techniques in the way they are normally implemented. One table is for both open regions (radiation and scattering problems), and another table is for guided wave problems. In this work, a novel recursive FDTD scheme is introduced, which relies on the piecewise polynomial functional dependence over $2\Delta t$, which is more rigorous than the piecewise linearization used by Kordi et al. [11], in calculating the convolution integral. Finally an equivalent model, using an equivalent single-conductor of a multiple conductor system is also established.

2. FORMULATION OF TRANSMISSION LINE EQUATIONS

The general layout of a system consisting of N overhead conductors located above a three-layer earth structure is shown in Fig. 1. The conductors of the same radius r are located at a position x_i and a height y_i $(i = 1,\ 2, \ldots, N)$ parallel to z-axis. The jth layer has permittivity $\varepsilon_j = \varepsilon_0\varepsilon_{rj}$ and conductivity σ_j. The air has a permeability μ_0 and permittivity ε_0 equal to those of the free space. All layers are of permeability $\mu_i = \mu_0$ $(i = 1, 2, 3)$. The 3rd layer is considered to be of infinite depth.

Assuming quasi-TEM mode of propagation, the overhead line depicted in Fig. 1 is described in the Laplace s-domain by the two matrix Equations (2) and (3), linking the voltages and currents of the line,

$$\frac{\partial \widetilde{\mathbf{I}}(z,\ s)}{\partial z} + \mathbf{Y}\widetilde{\mathbf{V}}(z,\ s) = 0 \tag{2}$$

$$\frac{\partial \widetilde{\mathbf{V}}(z,\ s)}{\partial z} + \mathbf{Z}\widetilde{\mathbf{I}}(z,\ s) = 0 \tag{3}$$

where $\widetilde{\mathbf{V}}$ is the voltage vector, $\widetilde{\mathbf{I}}$ the current vector, and z the longitudinal direction along the transmission line. Matrices $\mathbf{Z}$ and $\mathbf{Y}$ are the frequency dependent series impedance and shunt admittance per unit length matrices, respectively. s is the complex Laplace variable.

For the case of an overhead cable system, $\mathbf{Z}$ may be considered to consist of two components [11, 14]

$$\mathbf{Z} = \mathbf{Z}_w + \mathbf{Z}_e \tag{4}$$

where $\mathbf{Z}_w$ represents the per-unit-length internal impedances of the conductors in the cable system. For thin solid conductors, $\mathbf{Z}_w$ is defined as [15]

$$Z_{w,mn} \simeq \delta_{mn}\left(\frac{k_{wn}}{2\pi r\sigma_{wn}}\right)\frac{I_0(k_{wn}r)}{I_1(k_{wn}r)}, \quad \delta_{mn} = \begin{cases} 1, & m = n \\ 0, & m \neq n \end{cases}$$

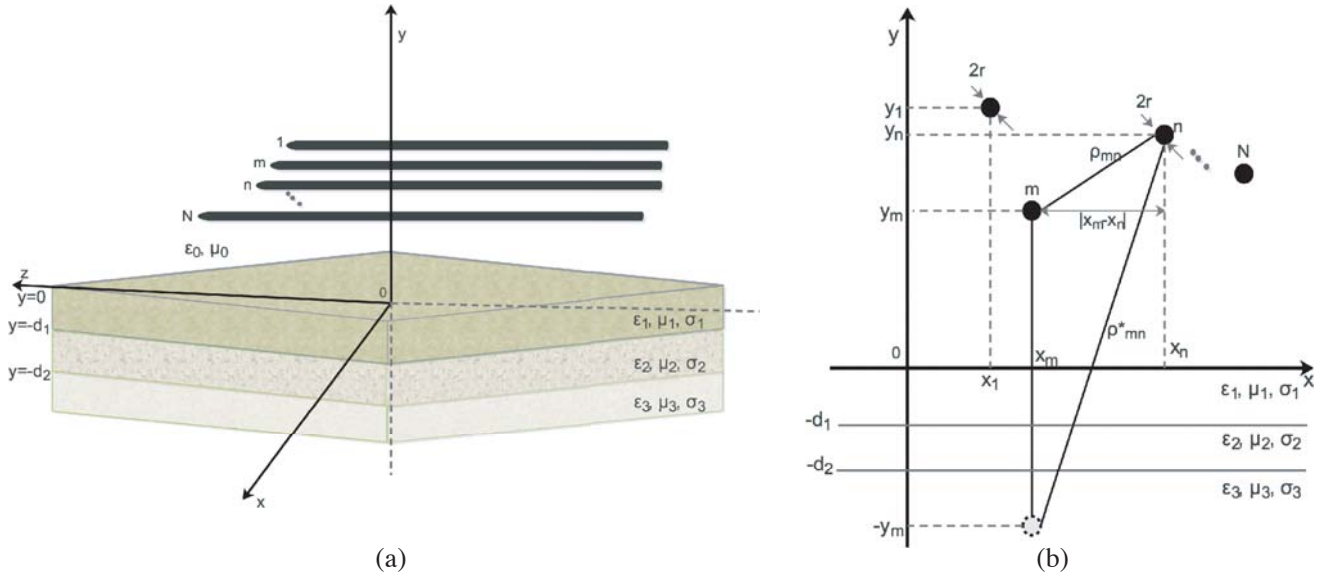

Figure 1. Geometry of multiconductor transmission line above a stratified earth. (a) Geometric configuration of overhead conductors. (b) Cross section of the wired structure.

where $k_{wn} = \sqrt{s\mu_{wn}(\sigma_{wn} + s\varepsilon_{wn})}$, and μ_{wn}, ε_{wn}, σ_{wn} are the electrical parameters characterizing the nth conductor. I_0, I_1 are the modified Bessel functions. $\mathbf{Z}_e$ accounts for the influence of the earth return path and is expressed as follows

$$\mathbf{Z}_e = s\mathbf{L} + \frac{s\mu_0}{\pi}\mathbf{J} \tag{5}$$

where $\mathbf{L}$ is the classical inductance matrix per unit length of the line whose elements are:

$$L_{mn} = \frac{\mu_0}{2\pi} \ln\left(\frac{\rho^*_{mn}}{\rho_{mn}}\right), \tag{6}$$

with $\rho_{mn} = \sqrt{(x_m - x_n)^2 + (y_m - y_n)^2}$ and $\rho^*_{mn} = \sqrt{(x_m - x_n)^2 + (y_m + y_n)^2}$. For a single conductor $\rho_{mn} = r$ and $\rho^*_{mn} = 2y_n\,(m = n)$. Matrix $\mathbf{J}$ represents the conduction losses in the ground. According to Nakagawa [6] model for the three-layer earth, $\mathbf{J}$ can be expressed as follows

$$J_{mn} = \int_0^\infty \chi^{(s)} e^{-(y_m + y_n)\nu} \cos(|x_m - x_n|\nu) d\nu \tag{7}$$

where

$$\begin{aligned}
\chi^{(s)} &= \frac{c_1 + c_2}{(\nu + \mu_0 b_1)c_1 + (\nu - \mu_0 b_1)c_2} \\
c_1 &= (b_1 + b_2)(b_2 + b_3) + (b_1 - b_2)(b_2 - b_3) \times e^{-2a_2(d_1 - d_2)} \\
c_2 &= \left((b_1 - b_2)(b_2 + b_3) + (b_1 + b_2)(b_2 - b_3) \times e^{-2a_2(d_1 - d_2)}\right) \times e^{-2a_1 d_1} \\
a_i &= \sqrt{v^2 + k_i^2 - k^2},\ b_i = a_i/\mu_i, \quad i = 1, 2 \text{ and } 3
\end{aligned} \tag{8}$$

In Eq. (8), k and $k_i = \sqrt{s\mu_i(\sigma_i + s\varepsilon_i)}$ ($i = 1, 2$ and 3) are the propagation constants in the air and in the ith layer, respectively.

The admittance matrix $\mathbf{Y}$ is generally expressed using a capacitive term and another one in integrals form representing displacement current losses in the earth. In most practical cases, whether for homogeneous or stratified soil, the displacement current in the soil is negligible compared to the conduction current [6, 16]. However, depending on the earth resistivity and conductor height, the admittance for the imperfectly conducting earth should be considered especially in a high-frequency

region when a transient involves a transition between TEM wave and TM/TE waves. Indeed, as indicated in [19], the return ground admittance due to a lossy ground affects the attenuation on conductors. At low frequencies, there is no difference between with and without the admittance correction including displacement current effect. When the frequency increases, the attenuation with the admittance correction starts to decrease due to the skin effect of the conductors at a critical frequency. This behavior corresponds to the transition between TEM and TM/TE modes, as Kikuchi pointed out in [20, 21]. This limits the used analytical earth return impedance model to only a few MHz. Other approaches, mainly the MOM-SO and FEM methods are used to overcome this limitation by correctly capturing skin, proximity, and ground effects, which are important factors for the analysis of the overhead line overvoltage [22]. Therefore, the quasi-TEM approach leads to the following well-known admittance used in steady-state and transient analysis on an overhead line [17]:

$$\mathbf{Y} \simeq s\varepsilon_0\mu_0\mathbf{L}^{-1} \tag{9}$$

3. IMPROVED FDTD ALGORITHM DERIVATION

In order to facilitate the transformation to the time domain of the transmission line equations a rational approximation of $\mathbf{Z}(s)$, which is based on the frequency response analysis data points, can be performed using the Vector Fitting (VF) algorithm presented by Gustavsen and Semlyen in [12]; thus, Eq. (4) can be fitted using a sum of M first order poles p_i with corresponding residues γ_i to reach the following expression

$$\mathbf{Z} = \mathbf{Z}'(s) + s(\mathbf{D} + \mathbf{L}) + \mathbf{R} \tag{10}$$

where

$$\mathbf{Z}'(s) = \sum_{i=1}^{M} \frac{\gamma_i}{(s - p_i)}$$

The residues γ_i and poles p_i are either real quantities or come in complex conjugate pairs, while $\mathbf{D}$ and $\mathbf{R}$ are a proportional term and a constant term, respectively. By inserting Eq. (10) in Eq. (3), the inverse Laplace transform of MTL equations can be expressed as follows:

$$\frac{\partial \mathbf{I}(z,t)}{\partial z} + \mathbf{C}\frac{\partial \mathbf{V}(z,t)}{\partial t} = 0 \tag{11}$$

$$\frac{\partial \mathbf{V}(z,t)}{\partial z} + (\mathbf{D} + \mathbf{L})\frac{\partial \mathbf{I}(z,t)}{\partial t} + \mathbf{R}\,\mathbf{I}(z,t) + \mathbf{Z}'(t) \circledast \mathbf{I}(z,t) = 0 \tag{12}$$

where $\mathbf{C} = \mu_0\epsilon_0\mathbf{L}^{-1}$, and the symbol $\circledast$ represents the convolution operator.

According to [11, 9], the convolution was performed using the time-domain derivative of the current instead of the current

$$\mathbf{Z}'(\tau) \circledast \mathbf{I}(z,t) = \int_0^t \mathbf{Z}'(\tau)d\tau \circledast \frac{\partial \mathbf{I}(z,t)}{\partial t} \tag{13}$$

By inserting Eq. (13) in Eq. (12) and evaluating the integral of $\mathbf{Z}'$, it is easy to show that

$$\frac{\partial \mathbf{V}(z,t)}{\partial z} + (\mathbf{L} + \mathbf{D})\frac{\mathbf{I}(z,t)}{\partial t} + (\mathbf{R} - \mathbf{\Omega})\mathbf{I}(z,t) + \phi(t) \circledast \frac{\partial}{\partial t}\mathbf{I}(z,t) = 0 \tag{14}$$

where

$$\mathbf{\Omega} = \sum_{i=1}^{M} \frac{\gamma_i}{p_i} \tag{15}$$

$$\phi = \sum_{i=1}^{M} \frac{\gamma_i}{p_i} e^{p_i t} \tag{16}$$

To solve the MTL Equations (11) and (14) directly in time domain, the FDTD method presented in [9, 11] is improved to solve the currents and voltages along the line. The transmission line is divided into K segments, each of length Δz. The current and voltage nodes are defined according to the discrete

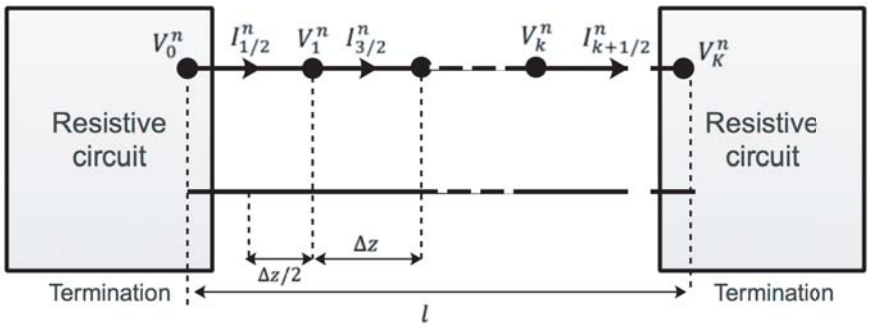

Figure 2. Voltage and current along the transmission line according to the discrete difference format π-type leapfrog.

difference format of π-type leapfrog as shown in Fig. 2. The current nodes are indicated by arrows, and voltage nodes are represented by dots. The distance between them is half the size, $\Delta z/2$. The two ends, separated by a length l, are supposed to be connected to resistive circuits.

The second-order time-space central difference approximations to Eqs. (11) and (14) lead to the following relationships

$$\frac{\mathbf{I}_{k+\frac{1}{2}}^{n+\frac{1}{2}} - \mathbf{I}_{k-\frac{1}{2}}^{n+\frac{1}{2}}}{\Delta z} + \mathbf{C}\frac{\mathbf{V}_k^{n+1} - \mathbf{V}_k^n}{\Delta t} = 0 \tag{17}$$

$$\frac{\mathbf{V}_{k+1}^n - \mathbf{V}_k^n}{\Delta z} + (\mathbf{L}+\mathbf{D})\frac{\mathbf{I}_{k+\frac{1}{2}}^{n+\frac{1}{2}} - \mathbf{I}_{k+\frac{1}{2}}^{n-\frac{1}{2}}}{\Delta t} + (\mathbf{R}-\mathbf{\Omega})\frac{\mathbf{I}_{k+\frac{1}{2}}^{n+\frac{1}{2}} + \mathbf{I}_{k+\frac{1}{2}}^{n-\frac{1}{2}}}{2}$$
$$+ \int_0^{n\Delta t} \phi(\tau)\frac{\partial}{\partial(n\Delta t-\tau)}\mathbf{I}_{k+\frac{1}{2}}(n\Delta t-\tau)d\tau = 0 \tag{18}$$

where k and n are the space and time indices, respectively. In order to obtain the transient current on an overhead line above a stratified earth, we need to solve Eq. (17) for $\mathbf{V}_k^{n+1}$, Eq. (18) for $\mathbf{I}_{k+\frac{1}{2}}^{n+\frac{1}{2}}$, and appropriately calculate the convolution integral given in Eq. (18).

In dealing with the convolution integral, previous formulations such as those presented in [9] and [11] have assumed that the time derivative of the current (TDC) at data point $k+1/2$ is either constant or linear over each time interval Δt. Greater accuracy can be achieved, however, if TDC is assumed to have a piecewise polynomial functional dependence over $2\Delta t$. In this work, the piecewise polynomial approximation to the continuous time derivative of the current over a given interval $[(m-1)\Delta t, (m+1)\Delta t]$ is expressed in terms of the time values $\partial_t \mathbf{I}_{k+\frac{1}{2}}(t-(m-1)\Delta t)$, $\partial_t \mathbf{I}_{k+\frac{1}{2}}(t-m\Delta t)$ and $\partial_t \mathbf{I}_{k+\frac{1}{2}}(t-(m+1)\Delta t)$ as

$$\frac{\partial}{\partial t}\mathbf{I}_{k+\frac{1}{2}}(t-\tau) = \frac{\partial}{\partial t}\mathbf{I}_{k+\frac{1}{2}}(t-m\Delta t) + \frac{\frac{\partial}{\partial t}\mathbf{I}_{k+\frac{1}{2}}(t-(m+1)\Delta t) - \frac{\partial}{\partial t}\mathbf{I}_{k+\frac{1}{2}}(t-(m-1)\Delta t)}{2\Delta t}(\tau - m\Delta t)$$
$$+ \frac{\frac{\partial}{\partial t}\mathbf{I}_{k+\frac{1}{2}}(t-(m+1)\Delta t) - 2\frac{\partial}{\partial t}\mathbf{I}_{k+\frac{1}{2}}(t-m\Delta t) + \frac{\partial}{\partial t}\mathbf{I}_{k+\frac{1}{2}}(t-(m-1)\Delta t)}{2\Delta t^2}(\tau - m\Delta t)^2 \tag{19}$$

Approximating the time derivatives of $\mathbf{I}_{k+\frac{1}{2}}$ in Eq. (19) with the central difference scheme at $n\Delta t$ and substituting the result into the convolution integral, considering definition of ϕ in Eq. (16), we get after some manipulation

$$\phi(t) \circledast \frac{\partial}{\partial t}\mathbf{I}_{k+\frac{1}{2}}(t)\Big|_{t=n\Delta t} = \sum_{i=1}^{M}\frac{\gamma_i}{p_i}\sum_{\substack{1\le m\le n,\\ m \text{ odd}}}(\mathbf{A}_m\chi_i^m + \mathbf{B}_m\xi_i^m + \mathbf{C}_m\eta_i^m) \tag{20}$$

where

$$\mathbf{A}_m = \mathbf{I}_{k+\frac{1}{2}}^{n-m+\frac{1}{2}} - \mathbf{I}_{k+\frac{1}{2}}^{n-m-\frac{1}{2}} \tag{21a}$$

$$\mathbf{B}_m = \mathbf{I}_{k+\frac{1}{2}}^{n-m-\frac{1}{2}} - \mathbf{I}_{k+\frac{1}{2}}^{n-m-\frac{3}{2}} - \mathbf{I}_{k+\frac{1}{2}}^{n-m+\frac{3}{2}} + \mathbf{I}_{k+\frac{1}{2}}^{n-m+\frac{1}{2}} \tag{21b}$$

$$\mathbf{C}_m = 3\mathbf{I}_{k+\frac{1}{2}}^{n-m-\frac{1}{2}} - \mathbf{I}_{k+\frac{1}{2}}^{n-m-\frac{3}{2}} + \mathbf{I}_{k+\frac{1}{2}}^{n-m+\frac{3}{2}} - 3\mathbf{I}_{k+\frac{1}{2}}^{n-m+\frac{1}{2}} \tag{21c}$$

In Eq. (21c), $\mathbf{I}_{k+\frac{1}{2}}^{n-m+j}$ stands for $\mathbf{I}((k+\frac{1}{2})\Delta z, (n-m+j)\Delta t),\ j = \pm\frac{1}{2}, \pm\frac{3}{2}$. The quantities χ_i^m, ξ_i^m and η_i^m are defined by

$$\chi_i^m = \frac{1}{\Delta t}\int_{(m-1)\Delta t}^{(m+1)\Delta t} e^{p_i\tau}\, d\tau \tag{21d}$$

$$\xi_i^m = \frac{1}{2\Delta t^2}\int_{(m-1)\Delta t}^{(m+1)\Delta t} e^{p_i\tau}(\tau - m\Delta t)\, d\tau \tag{21e}$$

$$\eta_i^m = \frac{1}{2\Delta t^3}\int_{(m-1)\Delta t}^{(m+1)\Delta t} e^{p_i\tau}(\tau - m\Delta t)^2\, d\tau \tag{21f}$$

and can be calculated recursively as

$$\chi_i^m = \frac{2e^{p_i m\Delta t}\sinh p_i\Delta t}{p_i\Delta t} \tag{22a}$$

$$\chi_i^m = e^{2p_i\Delta t}\chi_i^{m-2} \tag{22b}$$

$$\xi_i^m = \frac{e^{p_i m\Delta t}\Delta t(p_i\Delta t\cosh(p_i\Delta t) - \sinh(p_i\Delta t))}{(p_i\Delta t)^2} \tag{22c}$$

$$\xi_i^m = e^{2p_i\Delta t}\xi_i^{m-2} \tag{22d}$$

$$\eta_i^m = \frac{e^{p_i m\Delta t}\left(-2p_i\Delta t\cosh(p_i\Delta t) + \left(2 + (p_i\Delta)^2\right)\sinh(p_i\Delta t)\right)}{(p_i\Delta t)^2} \tag{22e}$$

$$\eta_i^m = e^{2p_i\Delta t}\eta_i^{m-2} \tag{22f}$$

Now, Eq. (20) can be rearranged in the following form

$$\phi(t) \circledast \frac{\partial}{\partial t}\mathbf{I}_{k+\frac{1}{2}}(t)\Big|_{t=n\Delta t} = \sum_{i=1}^{M}\frac{\gamma_i}{p_i}\left[\left(\mathbf{A}_1\chi_i^1 + \mathbf{B}_1\xi_i^1 + \mathbf{C}_1\eta_i^1\right) + \mathbf{\Psi}_i^n\right]$$

where

$$\mathbf{\Psi}_i^n = \sum_{\substack{m=3\\ m\ \text{odd}}}^{n}\left(\mathbf{A}_m\chi_i^m + \mathbf{B}_m\xi_i^m + \mathbf{C}_m\eta_i^m\right)$$

and

$$\mathbf{A}_1 = \mathbf{I}_{k+\frac{1}{2}}^{n-\frac{1}{2}} - \mathbf{I}_{k+\frac{1}{2}}^{n-\frac{3}{2}} \tag{23a}$$

$$\mathbf{B}_1 = \mathbf{I}_{k+\frac{1}{2}}^{n-\frac{3}{2}} - \mathbf{I}_{k+\frac{1}{2}}^{n-\frac{5}{2}} - \mathbf{I}_{k+\frac{1}{2}}^{n+\frac{1}{2}} + \mathbf{I}_{k+\frac{1}{2}}^{n-\frac{1}{2}} \tag{23b}$$

$$\mathbf{C}_1 = 3\mathbf{I}_{k+\frac{1}{2}}^{n-\frac{3}{2}} - \mathbf{I}_{k+\frac{1}{2}}^{n-\frac{5}{2}} + \mathbf{I}_{k+\frac{1}{2}}^{n+\frac{1}{2}} - 3\mathbf{I}_{k+\frac{1}{2}}^{n-\frac{1}{2}} \tag{23c}$$

Using Eqs. (22b), (22d), and (22f), a recursion relation for the quantity $\mathbf{\Psi}_i^n$ can be derived and is of the form

$$\begin{aligned}\mathbf{\Psi}_i^n = {} & \left(\mathbf{I}_{k+\frac{1}{2}}^{n-\frac{5}{2}} - \mathbf{I}_{k+\frac{1}{2}}^{n-\frac{7}{2}}\right)\chi_i^3 + \left(\mathbf{I}_{k+\frac{1}{2}}^{n-\frac{7}{2}} - \mathbf{I}_{k+\frac{1}{2}}^{n-\frac{9}{2}} - \mathbf{I}_{k+\frac{1}{2}}^{n-\frac{3}{2}} + \mathbf{I}_{k+\frac{1}{2}}^{n-\frac{5}{2}}\right)\xi_i^3 \\ & + \left(3\mathbf{I}_{k+\frac{1}{2}}^{n-\frac{7}{2}} - \mathbf{I}_{k+\frac{1}{2}}^{n-\frac{9}{2}} + \mathbf{I}_{k+\frac{1}{2}}^{n-\frac{3}{2}} - 3\mathbf{I}_{k+\frac{1}{2}}^{n-\frac{5}{2}}\right)\eta_i^3 + e^{2p_i\Delta t}\mathbf{\Psi}_i^{n-2}\end{aligned} \tag{24}$$

After calculating the above mentioned convolution integral, we can reach the solutions of the transmission line equations for $\mathbf{I}_{k+\frac{1}{2}}^{n+\frac{1}{2}}$ and $\mathbf{V}_k^{n+1}$. It is obvious to show that solutions for transient current and voltage are given by

$$\mathbf{I}_{k+\frac{1}{2}}^{n+\frac{1}{2}} = \mathbf{Z}_1^{-1}\left(\mathbf{Z}_2\mathbf{I}_{k+\frac{1}{2}}^{n-\frac{1}{2}} - \left(\mathbf{V}_{k+1}^{n} - \mathbf{V}_k^{n+1}\right) + \mathbf{Z}_3\mathbf{I}_{k+\frac{1}{2}}^{n-\frac{3}{2}} + Z_4\mathbf{I}_{k+\frac{1}{2}}^{n-\frac{5}{2}} - \Delta z\boldsymbol{\Psi}^n\right) \tag{25}$$

where

$$\begin{aligned}
\mathbf{Z}_1 &= \Delta z\left(\frac{\mathbf{L}+\mathbf{D}}{\Delta t} + \frac{\mathbf{R}}{2} - \frac{\boldsymbol{\Omega}}{2} - \xi + \eta\right)\\
\mathbf{Z}_2 &= \Delta z\left(\frac{\mathbf{L}+\mathbf{D}}{\Delta t} - \frac{\mathbf{R}}{2} + \frac{\boldsymbol{\Omega}}{2} - \chi - \xi + 3\eta\right)\\
\mathbf{Z}_3 &= \Delta z(\chi - \xi - 3\eta)\\
\mathbf{Z}_4 &= \Delta z(\xi + \eta)\\
\chi &= \sum_{i=1}^{M}\frac{\gamma_i}{p_i}\chi_i^1\\
\xi &= \sum_{i=1}^{M}\frac{\gamma_i}{p_i}\xi_i^1\\
\eta &= \sum_{i=1}^{M}\frac{\gamma_i}{p_i}\eta_i^1\\
\boldsymbol{\Psi}^n &= \sum_{i=1}^{M}\frac{\gamma_i}{p_i}\boldsymbol{\Psi}_i^n
\end{aligned} \tag{26}$$

and

$$\mathbf{V}_k^{n+1} = \mathbf{V}_k^n - \frac{1}{\varepsilon_0\mu_0}\left(\frac{\Delta t}{\Delta z}\right)\mathbf{L}\ \left(\mathbf{I}_{k+\frac{1}{2}}^{n+\frac{1}{2}} - \mathbf{I}_{k+\frac{1}{2}}^{n-\frac{1}{2}}\right) \tag{27}$$

The FDTD scheme used to discretize the MTL equations cannot be adapted to the terminal voltages, because the voltages and currents at each end have not been given by the solution listed above, i.e., the solutions for $\mathbf{V}_0$ and $\mathbf{V}_K$ remain to be defined. It is assumed that the sending end of the line is connected with a voltage source whose voltage is $\mathbf{E}_s$, and internal resistance is $\mathbf{R}_0$. Similarly, resistive load $\mathbf{R}_L$ is assumed to be connected to the receiving end. According to the technique used in [9], the terminal condition can be written as

$$\mathbf{V}_1^{n+1} = \mathbf{G}_1^{-1}\left(\mathbf{G}_2\mathbf{V}_0^n - \frac{2}{\Delta z}\mathbf{I}_{\frac{1}{2}}^{n+\frac{1}{2}} + \frac{\mathbf{R}_0^{-1}\mathbf{E}_s}{\Delta z}\right)$$

and

$$\mathbf{V}_K^{n+1} = \mathbf{Y}_1^{-1}\left(\mathbf{Y}_2\mathbf{V}_K^n + 2\frac{\mathbf{I}_K^{n-\frac{1}{2}}}{\Delta z}\right)$$

where

$$\begin{aligned}
\mathbf{G}_1 &= \frac{\mathbf{C}}{\Delta t} + \frac{\mathbf{R}_0^{-1}}{\Delta z}\\
\mathbf{G}_2 &= \frac{\mathbf{C}}{\Delta t} - \frac{\mathbf{R}_0^{-1}}{\Delta z}\\
\mathbf{Y}_1 &= \frac{\mathbf{C}}{\Delta t} + \frac{\mathbf{R}_L^{-1}}{\Delta z}\\
\mathbf{Y}_2 &= \frac{\mathbf{C}}{\Delta t} - \frac{\mathbf{R}_L^{-1}}{\Delta z}
\end{aligned}$$

4. RESULTS AND DISCUSSION

In this part, we will check the validity of the proposed method. As a first illustrative example, we consider an overhead line consisting of three conductors of the same radius $r = 2.5\,\text{mm}$ placed above two-layer soil as shown in Fig. 3. The upper layer height and its relative permittivity are set at $d = 1\,\text{m}$ and $\varepsilon_{r1} = 10$. The bottom layer permittivity ε_{r2} is equal to 8. Conductors 1 and 3 are located at the same height $y_{1,3} = 10\,\text{m}$ and are 5 m apart. Conductor 2 is placed at 2.5 m of conductor 1 to the height $y_2 = 12\,\text{m}$. The loads are $\mathbf{R}_0 = \text{diag}(100, 50)\,\Omega$, $\mathbf{R}_L = \text{diag}(100, 100)\,\Omega$. Figs. 4(a), (b) illustrate the effect of two-layer earth conductivity ratio on the impedance $Z_{L11} = (\mathbf{Z} - \mathbf{L}j\omega)_{11}$ by adopting the Nakagawa and Sunde models. It is worth noting that the Nakagawa two-layer model is obtained from Equation (8) by putting $c_1 = b_1 + b_2$, $c_2 = (b_1 - b_2)\exp(-2a_1d_1)$. The figure shows that Nakagawa and Sunde models agree with a slight difference towards the high frequencies. In addition, when the conductivity of the upper layer is greater than that of the lower layer ($\frac{\sigma_1}{\sigma_2} = 100$), the penetration depth of the return current is greater at low frequencies. Consequently, the lower the ratio of first

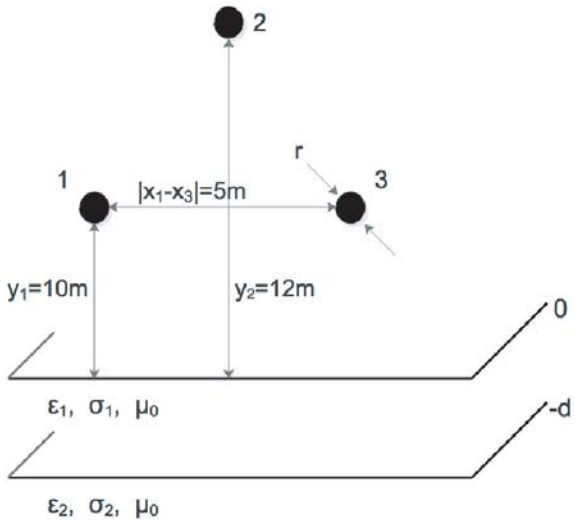

Figure 3. Three-conductor overhead line configuration.

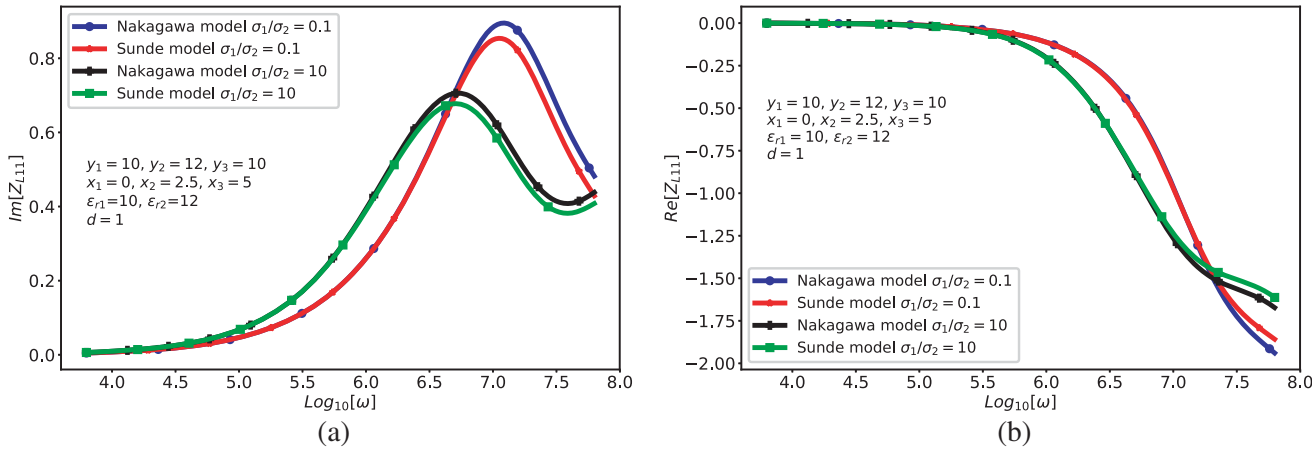

Figure 4. Effect of two-layer earth conductivity ratio on $Z_{L_{11}}(j\omega) = (\mathbf{Z}(j\omega) - \mathbf{L}j\omega)_{11}$ for Nakagawa and Sunde models. (a) $\text{Im}(Z_{L_{11}}(j\omega))$. (b) $\text{Re}(Z_{L_{11}}(j\omega))$.

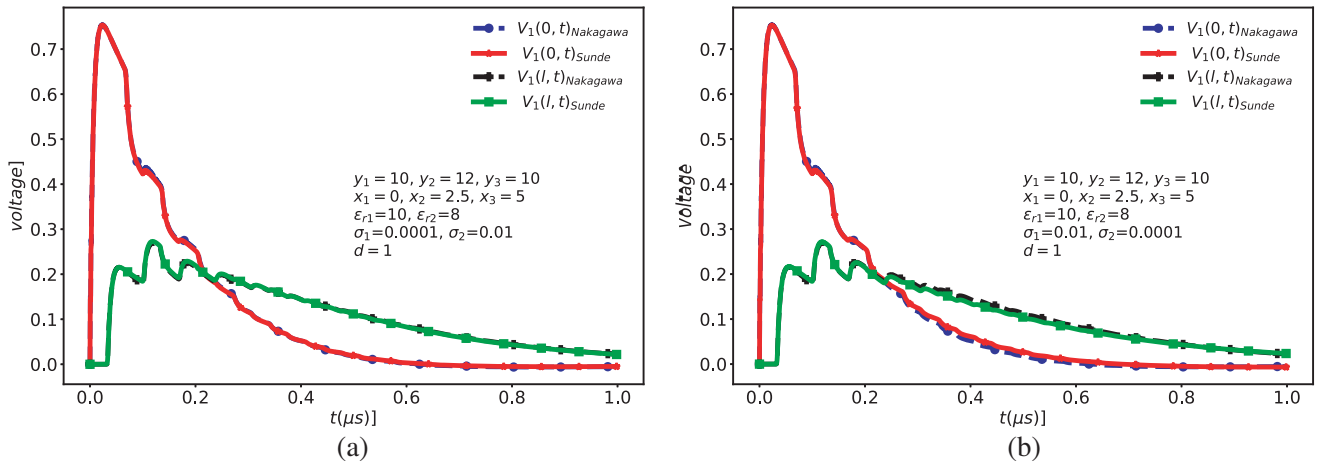

Figure 5. Effect of two-layer earth conductivity ratio on the conductor 1's voltage for Nakagawa and Sunde models. (a) For $\sigma_1 < \sigma_2$. (b) For $\sigma_1 > \sigma_2$.

to lower-layer conductivity is, the lower the conduction losses are (see the result for $\frac{\sigma_1}{\sigma_2} = 0.01$). At high frequencies, the penetration depth becomes smaller and smaller, and conduction losses increase for $\sigma_1 < \sigma_2$. The difference between the two models influence on the voltage response as shown in Fig. 5 is more noticeable for the case when $\sigma_1 > \sigma_2$ (see Figure 5(b)).

In the second example, we consider a three-conductor overhead line referred to as three-conductor model (TCM). The conductors are located above a three-layer earth characterized by the conductivities $\sigma_1 = 0.0001\,\mathrm{S/m}$, $\sigma_2 = 0.001\,\mathrm{S/m}$ and $\sigma_3 = 0.01\,\mathrm{S/m}$, the relative permittivities $\varepsilon_{r1} = 10$, $\varepsilon_{r2} = 8$ and $\varepsilon_{r3} = 5$, and the positions of the layer interfaces $d_1 = 1\,\mathrm{m}$, $d_2 = 3\,\mathrm{m}$. Details of geometric parameters of the conductors are shown in Fig. 6(a). Fig. 6(b) shows the equivalent two-conductor line (ETCM)

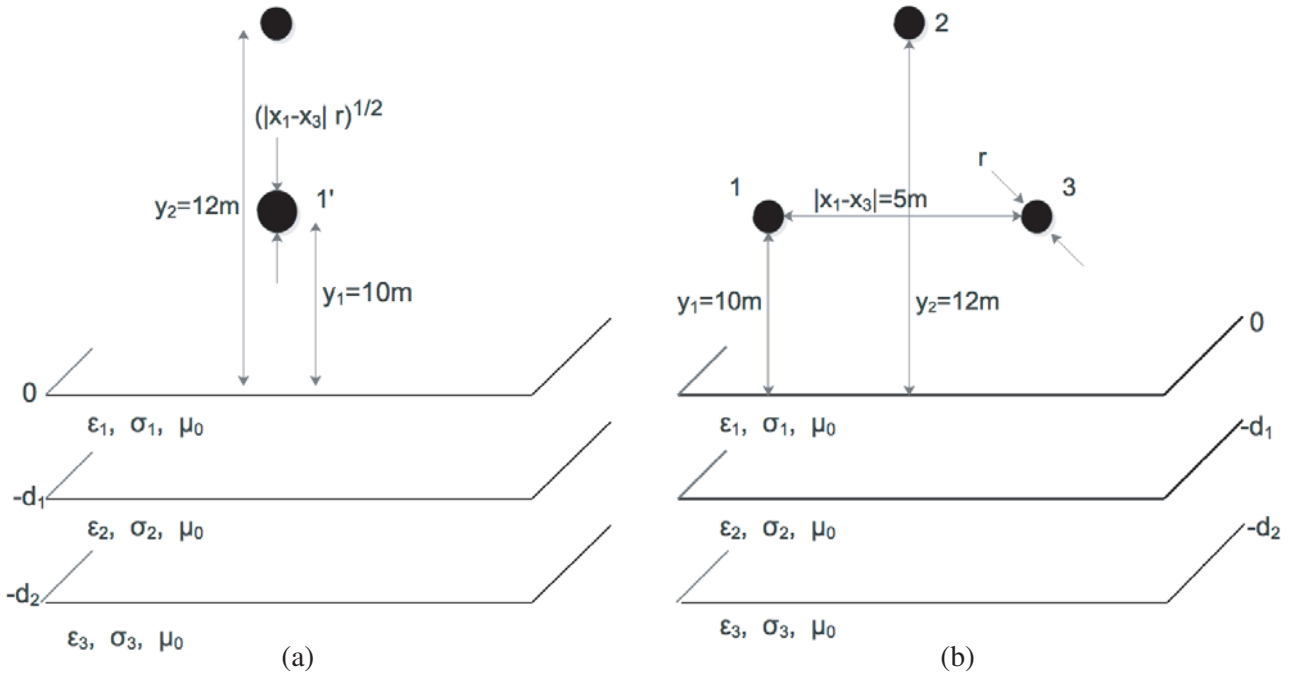

Figure 6. (a) Three-conductor transmission line configuration (TCM). (b) Equivalent two-conductor transmission line (ETCM).

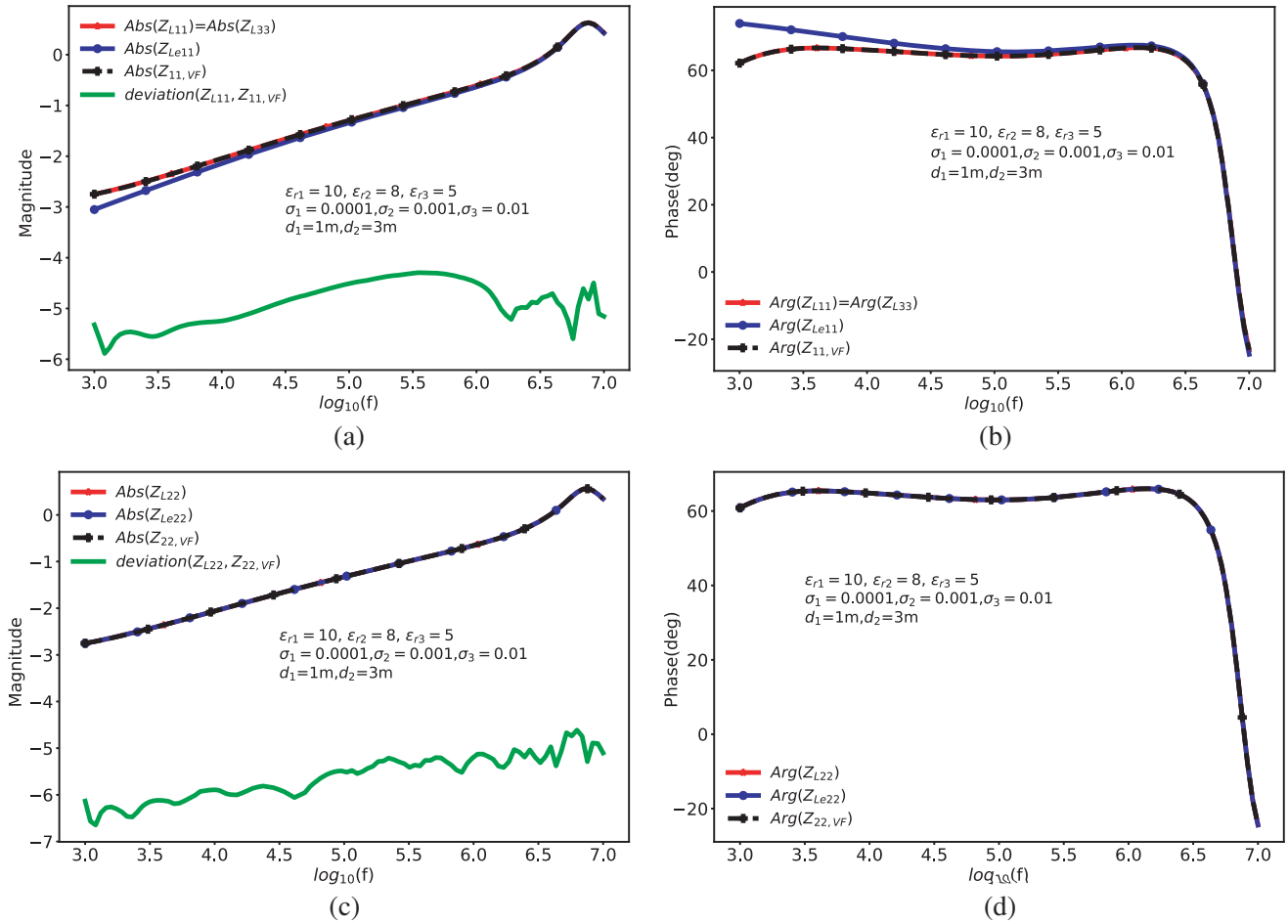

Figure 7. Comparison between Z_L for TCM and ETCM.

of the TCM obtained by replacing the two conductors at $y_{1,3} = 10\,\text{m}$ above the ground with a single equivalent conductor $1'$ of the radius $r_{eq} = \sqrt{r|x_1 - x_3|} = 0.112\,\text{m}$ placed halfway between conductors 1 and 3.

Figure 7 shows the comparison between the TCM and ETCM models. Figs. 6(a) and 6(b) show the frequency variation of the magnitude (in decibels) and phase of the impedance $Z_{L11}(j\omega) = Z_{L33}(j\omega)$ respectively for the three-conductor line as well as the deviation between the exact model and the result obtained by the vector fitting $|Z_{L11} - Z_{L11,VF}|$ in decibels. Also, the variation as a function of the frequency of the impedance $Z_{Le11}(j\omega)$ of the two-conductor line is shown in Figs. 6(a) and 6(b). The same variations are reproduced in Figs. 6(c) and 6(d), but with respect to the impedances $Z_{L22}(j\omega)$ and $Z_{Le22}(j\omega)$. From the examination of these curves, it emerges that the reduced two-conductor model is able to efficiently model the three-conductor structure, particularly the impedance of conductor 2. For conductor 1, a slight deviation is observed at low frequencies between the two models.

Now, in the three-conductor line configuration of Fig. 5(a), the sending end is connected to the source whose voltage is $\mathbf{E}_s = (e_d(t), e_d(t - t_0), e_d(t))$, where $e_d(t)$ is assumed to be a double exponential waveform given by

$$e_d(t) = E_0 \left(e^{-\alpha t} - e^{-\beta t}\right)$$

with $\alpha = 4.01 \times 10^6 s^{-1}$, $\beta = 4.76 \times 10^8\,\text{s}^{-1}$, and $E_0 = 1\,\text{V}$. Note that the excitation source of the second conductor for the TCM model is shifted by $t_0 = 0.1\,\mu\text{s}$. The internal resistance of the source and the load are respectively set at $\mathbf{R}_0 = \text{diag}(100, 50, 100)\Omega$ and $\mathbf{R}_L = \text{diag}(100, 100, 100)\Omega$, where diag stands for the diagonal matrix. For the equivalent two-conductor line for Fig. 5(b), the internal voltage source

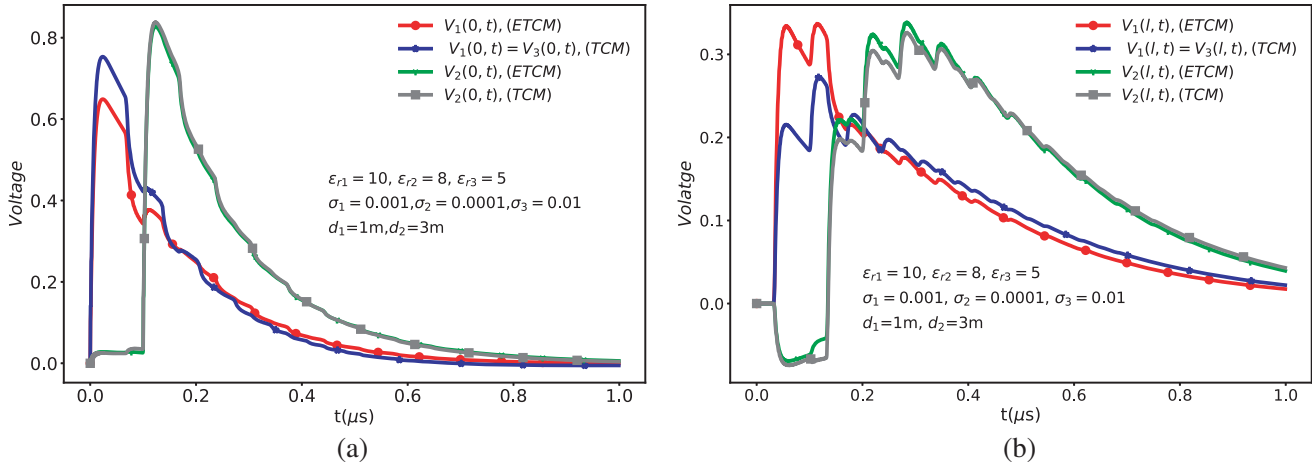

Figure 8. Voltages for TCM and ETCM. (a) Near end. (b) Far end.

is $\mathbf{E}_{se} = (e_d(t),\ e_d(t - t_0))$, and the loads are $\mathbf{R}_{0e} = \text{diag}(100, 50)\Omega$, $\mathbf{R}_{Le} = \text{diag}(100, 100)\Omega$. Fig. 8 shows the voltages at the near ($z = 0\,\text{m}$) and far ($z = 10\,\text{m}$) ends for TCM and ETCM models. Here, we find the same result concerning the reduced equivalent two-conductor line model of the TCM, i.e., it allows to accurately reproduce the voltage on conductor 2 at both the near and far ends. Note that this is valid when conductors 1 and 3 have identical characteristics and identical sources and loads. The use of the ETCM is particularly interesting, it allows us to reduce the number of conductors by replacing conductors 1 and 3 (TCM) that are located in the same height by an equivalent conductor without influencing the voltage on conductor 2.

5. CONCLUSION

In this paper, the transient response of an overhead line in the presence of stratified earth has been established. To achieve this, a new finite difference algorithm is developed, based on an improvement in the calculation of the usual convolution integral between the time derivative of the current and the ground return impedance. The Nakagawa model is adopted for this impedance, which is then approximated by a sum of exponential functions obtained by the frequency-domain vector fitting method. Finally, the equivalent model of replacing two identical parallel conductors, placed at the same height above the ground, by a single conductor, remains a very effective way of reducing the complexity of the wired structure while providing a very good estimate of the transient voltages.

REFERENCES

1. Carson, J. R., "Wave propagation in overhead wires with ground return," *Bell Syst. Tech. J.*, Vol. 5, 539–554, 1926.
2. Pollaczek, F., "Uber das feld einer unerdlich langen wechselstrom-durchflossenen Einfachleitung," *Elect. Nachr. Tech.*, Vol. 9, 339, 1926.
3. Wise, W. H., "Propagation of high frequency currents in ground return circuits," *Proc. Inst. Radio Eng.*, Vol. 22, 522–527, 1934.
4. Sunde, E. D., *Earth Conduction Effects in Transmission Systems*, 99–139, 2nd Edition, Dover Publications, 1968.
5. Papadopoulos, T. A., K. Papagiannis, and D. P. Labridis, "A generalized model for the calculation of the impedances and admittances of overhead power lines above stratified earth," *Electric Power Systems Research*, Vol. 80, 1160–1170, 2010.

6. Nakagawa, N., A. Ametani, and K. Iwamoto, "Further studies on wave propagation in overhead lines with earth return: Impedance of stratified earth," *Proc. IEE*, Vol. 120, No. 12, 1521–1528, 1973.
7. Agrawal, A. K., H. J. Price, and S. H. Gurbaxani, "Transient response of multiconductor transmission line excited by a nonuniform electromagnetic field," *IEEE Transactions on Electromagnetic Compatibility*, Vol. 22, 119–129, 1980.
8. Djorjevic, A. R., T. S. Sarkar, and R. F. Harrington, "Time domain response of multiconductor transmission lines," *Proc. IEEE*, Vol. 75, No. 6, 119–764, June 1987.
9. Paul, C. R., *Analysis of Multiconductor Transmission Lines*, Ch. 5, New York, Wiley, 1994.
10. Rachidi, F., C. A. Nucci, and M. Ianoz, "Transient analysis of multiconductor lines above a lossy ground," *IEEE Trans. Electromagn.*, Vol. 14, No. 1, January 1999.
11. Kordi, B., J. Lovetri, and G. E. Bridges, "Finite-difference analysis of dispersive transmission lines within a circuit simulator," *IEEE Trans. Electromagn. Compat.*, Vol. 21, No. 1, January 2006.
12. Gustavsen, B. and A. Semlyen, "Rational approximation of frequency-domain responses by vector fitting," *IEEE Trans. Power Del.*, Vol. 14, No. 3, 1052–1061, July 1999.
13. Yee, K., "Numerical solution of initial boundary value problems involving Maxwell's equations in isotropic media," *IEEE Transactions on Antenaas and Propagation*, Vol. 14, 302–307, 1966.
14. Belganche, Z., A. Maaouni, A. Mzerd, and A. Bouziane, "Equivalent model from two layers stratified media to homogeneous media for overhead lines," *Progress In Electromagnetics Research M*, Vol. 41, 63–72, 2015.
15. Stratton, J. A., *Electromagnetic Theory*, McGraw-Hill, New York, 1941.
16. Bridges, G. E. J. and L. Shafai, "Plane wave coupling to multiple conductor transmission lines above a lossy earth," *IEEE Trans. On Electromagn. Compat.*, Vol. 31, No. 1, 21–33, February 1989.
17. Ametani, A., N. Nagaoka, Y. Baba, T. Ohno, and K. Yamabuki, *Power System Transients: Theory and Applications*, CRC Press, 2013.
18. Davidson, D. B., *Computational Electromagnetics for RF and Microwave Engineering*, 6–7, Cambridge University Press, Cambridge, United Kingdom, 2005.
19. Nakagawa, M., "Further studies on wave propagation along overhead transmission lines: Effect of admittance correction," *IEEE Transactions on Power Apparatus and Systems*, Vol. 100, July 1981.
20. Kikuchi, H., "Electromagnetic field on infinite wire at high frequencies above plane-wave," *IEE Japan*, Vol. 77, No. 825, 721–733, 1959.
21. Kikuchi, H., "Wave propagation on the ground return circuit in high frequency regions," *J. IEE Japan*, Vol. 75, No. 805, 1176–1187, 1955.
22. Borecki, M., J. Starzyski, and Z. Krawczyk, "The comparative analysis of selected overvoltage protection measures for medium voltage overhead lines with covered conductors," *Progress in Applied Electrical Engineering (PAEE)*, 1–4. 2017.